



HAL
open science

Mixing and recirculation characteristics of gas-liquid Taylor flow in microreactors

Thomas Abadie, Catherine Xuereb, Dominique Legendre, Joelle Aubin

► **To cite this version:**

Thomas Abadie, Catherine Xuereb, Dominique Legendre, Joelle Aubin. Mixing and recirculation characteristics of gas-liquid Taylor flow in microreactors. *Chemical Engineering Research and Design*, 2013, 91 (11), pp.2225-2234. 10.1016/j.cherd.2013.03.003 . hal-03524803

HAL Id: hal-03524803

<https://hal.science/hal-03524803>

Submitted on 13 Jan 2022

HAL is a multi-disciplinary open access archive for the deposit and dissemination of scientific research documents, whether they are published or not. The documents may come from teaching and research institutions in France or abroad, or from public or private research centers.

L'archive ouverte pluridisciplinaire **HAL**, est destinée au dépôt et à la diffusion de documents scientifiques de niveau recherche, publiés ou non, émanant des établissements d'enseignement et de recherche français ou étrangers, des laboratoires publics ou privés.



Open Archive TOULOUSE Archive Ouverte (OATAO)

OATAO is an open access repository that collects the work of some Toulouse researchers and makes it freely available over the web where possible.

This is an author's version published in : <http://oatao.univ-toulouse.fr/9907>

Official URL : <https://doi.org/10.1016/j.cherd.2013.03.003>

To cite this version :

Abadie, Thomas  and Xuereb, Catherine  and Legendre, Dominique 
and Aubin, Joelle  *Mixing and recirculation characteristics of gas-liquid Taylor flow in microreactors* (2013) *Chemical Engineering Research and Design*, vol. 91 (n°11). pp. 2225-2234. ISSN 0263-8762

Any correspondence concerning this service should be sent to the repository administrator :
tech-oatao@listes-diff.inp-toulouse.fr

Mixing and recirculation characteristics of gas–liquid Taylor flow in microreactors

T. Abadie^{a,b}, C. Xuereb^b, D. Legendre^{a,**}, J. Aubin^{b,*}

^a University of Toulouse, Institut de Mécanique des Fluides CNRS/INPT/UPS, 1 Allée du Professeur Camille Soula, 31400 Toulouse, France

^b University of Toulouse, Laboratoire de Génie Chimique CNRS/INPT/UPS, 4 Allée Emile Monso, BP-84234, 31030 Toulouse, France

A B S T R A C T

The effects of operating parameters (capillary and Reynolds numbers) and microchannel aspect ratio ($\alpha = w/h = [1; 2.5; 4]$) on the recirculation characteristics of the liquid slug in gas–liquid Taylor flow in microchannels have been investigated using 3-dimensional VOF simulations. The results show a decrease in the recirculation volume in the slug and an increase in recirculation time with increasing capillary number, which is in good agreement with previous results obtained in circular and square geometries (Thulasidas et al., 1997). In addition, increasing the aspect ratio of the channel leads to a slight decrease in recirculating volumes but also a significant increase in recirculation times.

Keywords: Gas–liquid Taylor flow; Microchannel; Microreactor; Mixing; Recirculation; CFD; VOF

1. Introduction

Over the last decade, micro reaction technology has become of much interest to both academics and the process industries for the intensification of chemical processes. Taylor or slug flow is a commonly encountered flow regime for gas–liquid microchannel flows and has the advantage of providing high interfacial area and good liquid mixing in the liquid slug, thereby enhancing transport processes. These features of microreactors are particularly interesting for fast and highly exothermic gas–liquid reactions – amongst other applications – and allow an increase in reaction performance whilst working under safe operating conditions (Hessel et al., 2005; Kashid and Kiwi-Minsker, 2009). A number of studies have focused on the understanding of hydrodynamics as well as heat and mass transfer enhancement in these flows (see reviews Kreutzer et al., 2005; Shao et al., 2009; Gupta et al., 2010) but often independently. Indeed the transport efficiency appears to be closely related to the recirculation in the liquid phase, which depends on the operating conditions, fluid properties and reactor geometry.

A major feature of gas–liquid Taylor flow is the recirculation flow pattern generated in the liquid slug in the moving frame

of reference as shown in Fig. 1 and detailed by Taylor (1961). The recirculating flow pattern is characterized by the position of the center of the circulation loop $[x_0, y_0]$, and the position of the streamline separating the recirculation zone and the liquid film at the channel wall $[x_1, y_1]$. As the bubble velocity increases, both the loop center and the outer streamline of the recirculation zone move towards the center of the channel (Thulasidas et al., 1997). This leads to a reduction of the volume of the recirculating zone and an increase in the volume of liquid in the film region until complete bypass flow occurs at $U_B \geq U_{max}$. Studies on the recirculating flow in circular and square capillaries have been conducted previously (Taylor, 1961; Thulasidas et al., 1997), however little information on the characteristics of the recirculation zone in rectangular channels is available. Recently, it has been shown theoretically (Kececi et al., 2009) that the cross-sectional area occupied by the recirculation zone in the liquid slug is generally smaller for rectangular channels than for circular channels due to the increased film thickness in the channel corners.

The recirculation time in the liquid slug in Taylor flow is defined as the time required for an element of fluid to complete one revolution in the recirculating slug. This characteristic time is particularly relevant for transport processes

* Corresponding author. Tel.: +33 534323714.

** Corresponding author. Tel.: +33 534322818.

E-mail addresses: dominique.legendre@imft.fr (D. Legendre), joelle.aubincano@ensiacet.fr (J. Aubin).

<http://dx.doi.org/10.1016/j.cherd.2013.03.003>

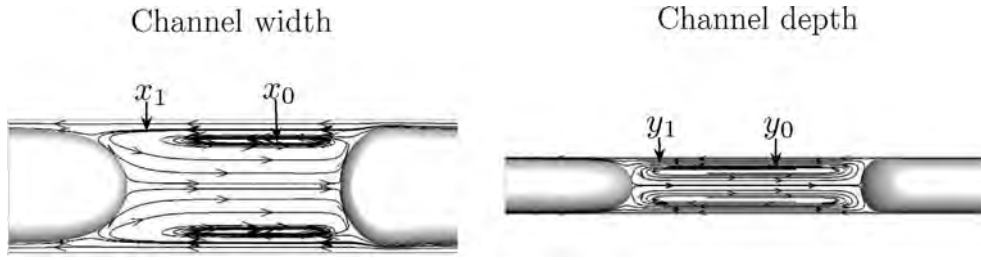


Fig. 1 – Streamline pattern in the frame of reference moving with the bubble ($Ca = 0.06$ and $Re = 16.8$). The flow is directed from the left to the right. The positive part of the recirculating pattern of volume V_0 is delimited by the coordinates $[x_0, y_0]$ in the channel width and depth; the negative part of the recirculating zone of volume $V_1 = V_{rc} - V_0$ is located between $[x_0, y_0]$ and $[x_1, y_1]$; and the film region of volume $V_2 = V_{slug} - V_{rc}$ is located between $[x_1, y_1]$ and the walls.

occurring in the system, such as mass transfer between the bubble and slug or wall and slug, and heat transfer with the channel wall. The rate of flow recirculation can be calculated via the surface integration of the relative velocity profile across the microchannel cross-section, similarly to what is done in conventional stirred tanks to calculate circulation induced by the mechanical impeller [Jaworski et al. \(1996\)](#). The recirculation flow rate through the microchannel can be divided into three parts (illustrated in [Fig. 1](#)):

- a positive flow rate, Q_0 , in the main flow direction at central core of the microchannel occupying a volume V_0 with a cross-sectional area A_0 ,
- a negative flow rate, Q_1 , with a volume V_1 and a cross-sectional area A_1 that corresponds to the recirculating liquid in the slug,
- a negative flow rate, Q_2 of volume V_2 in area A_2 , that is close to the channel wall and contributes to axial mixing between slugs instead of radial mixing within the slug.

The recirculation time is then defined as $t_{rc} = V_{rc}/Q_{rc}$, where the recirculating volume V_{rc} corresponds to the volume of liquid within the limit of the separating streamline and Q_{rc} is the recirculation flow rate equal to Q_0 (and $|Q_1|$). t_{rc} can be made non dimensional by dividing it by the time taken for the bubble to travel a distance equal to the slug length: $\tau_{rc} = t_{rc}/(L_S/U_B)$.

In our previous work we have explored the effects of fluid properties, operating conditions and microchannel geometry on the size of Taylor bubbles ([Abadie et al., 2012](#)) and the flow patterns in the liquid slug using micro Particle Image Velocimetry (μ -PIV) ([Zaloha et al., 2012](#)). The objective of this work is to explore the effects of operating parameters (capillary, Ca , and Reynolds numbers, Re) and microchannel aspect ratio ($\alpha = w/h = [1; 2.5; 4]$) on the mixing and recirculation characteristics of the liquid slug in gas-liquid Taylor flow in microchannels. To do this, 3-dimensional VOF simulations of gas-liquid Taylor flow in microchannels have been performed. Using an approach that is analogous to the determination of circulation rate in stirred tanks, the recirculation rate in the liquid slug, as well as the size of the recirculating zone have been evaluated from the 3-dimensional numerical data. An attempt has been made to relate these characteristics of the recirculating liquid slug to the enhanced transport phenomena observed in Taylor flow in microreactors. Finally, recommendations on the design and operation of microreactors employing Taylor flow are given.

2. Methodology

2.1. Theoretical developed velocity profile in rectangular capillaries

In the limit of infinite slug length, the analytical solution of the velocity profile in a cross-section of a rectangular capillary can be derived. The corresponding velocity profile in a rectangular capillary with a cross-section $2w \times 2h$ is given by Eqs. (1) and (2). This theoretical velocity profile has been used to evaluate the effects of aspect ratio and dimensionless bubble velocity on characteristic parameters of recirculation motion in gas-liquid Taylor flow: recirculating volumes and recirculation times. Under the assumption that the slug is long when compared with development lengths of velocity profile at the rear and the nose caps of the bubbles, the recirculation volume can be approximated by the cross-sectional area of the recirculating zone multiplied by the slug length: $V_{0,1} \sim A_{0,1} \times L_S$.

$$u(x, y) = -\frac{16c_1 w^2}{\pi^3} \sum_{n=1,3,\dots}^{\infty} \frac{-1^{(n-1)/2}}{n^3} \left[1 - \frac{\cosh(n\pi y/2w)}{\cosh(n\pi h/2w)} \right] \cos\left(\frac{n\pi x}{2w}\right) \quad (1)$$

$$U_{TP} = -\frac{c_1 w^2}{3} \left[1 - \frac{192 w}{\pi^5 h} \sum_{n=1,3,\dots}^{\infty} \frac{1}{n^5} \tanh\left(\frac{n\pi h}{2w}\right) \right] \quad (2)$$

Numerical integration of the profiles (1) and (2) for aspect ratios $\alpha = [1; 2.5; 4]$ have been performed on fine uniform grids of 400×400 , 1000×400 and 1600×400 , respectively, to calculate the area A_0 where the velocity in the moving coordinate system is positive. Following this, an iterative integration of A_1 (cross-section of the negative part of the recirculating liquid) has been performed until the flow rates in the positive and negative parts of the recirculating zone are balanced. Integration of these profiles allows the prediction of recirculating volumes and recirculation times as a function of the aspect ratio and the dimensionless velocity $W = (U_B - U_{TP})/U_B$ assuming long liquid slugs.

2.2. Numerical simulations

The numerical code used for this study is the JADIM code, which has been developed to simulate dispersed two-phase flows and used to simulate various multiphase flows systems ([Bonometti and Magnaudet, 2007](#); [Dupont and Legendre, 2010](#); [Sarrazin et al., 2006a,b](#); [Abadie et al., 2012](#)). The interface capturing technique implemented in this code is the Volume of Fluid method (VOF), which consists of a Eulerian description of each phase on a fixed grid. Under the assumptions that (i) the fluids are Newtonian and incompressible, (ii) there is no mass

transfer at the interface, (iii) the flow is isothermal and (iv) the surface tension is constant, the fluid flow can be described by the classical one fluid formulation of the Navier–Stokes equations:

$$\nabla \cdot \mathbf{U} = 0 \quad (3)$$

$$\rho \left(\frac{\partial \mathbf{U}}{\partial t} + (\mathbf{U} \cdot \nabla) \mathbf{U} \right) = -\nabla P + \nabla \cdot \boldsymbol{\Sigma} + \rho \mathbf{g} + \mathbf{F}_{\sigma,s} \quad (4)$$

where $\boldsymbol{\Sigma}$ is the viscous stress tensor, \mathbf{g} is the acceleration due to gravity, $\mathbf{F}_{\sigma,s} = -\sigma (\nabla \cdot \mathbf{n}) \mathbf{n} \delta_I$ is the capillary contribution whose calculation is described below, σ is the surface tension, \mathbf{n} the normal to the interface, δ_I is the Dirac distribution localizing the interface, and ρ and μ are the local density and dynamic viscosity, respectively. The density and viscosity are deduced from the volume fraction of one phase (or color function) C by linear interpolation:

$$\rho = C\rho_1 + (1 - C)\rho_2, \quad \mu = C\mu_1 + (1 - C)\mu_2 \quad (5)$$

where the volume fraction is $C=1$ in cells filled with fluid 1, $C=0$ in cells filled with fluid 2 and $0 < C < 1$ in cells that are cut by the interface. Additionally, the transport equation of the color function is solved to capture the interface between the phases:

$$\frac{\partial C}{\partial t} + \mathbf{U} \cdot \nabla C = 0 \quad (6)$$

In many VOF methods employed to capture a fluid–fluid interface, a reconstruction technique is used to control the thickness of the interface. In the *JADIM* code, the location and thickness of the interface are both controlled by an accurate algorithm based on Flux-Corrected Transport schemes (Zalesak, 1979; Bonometti and Magnaudet, 2007).

The equations are discretized on a staggered grid using a finite volume method and all spatial derivatives are approximated using second-order centered schemes. The time scheme used to compute the advective terms in the Navier–Stokes equations is a third-order Runge–Kutta type scheme, while the viscous stresses are solved using a semi-implicit Crank–Nicolson method. The incompressibility is ensured using a projection method, which consists in splitting the velocity field into two contributions: a rotational one, which gives a predicted velocity field calculated semi-implicitly, and a potential one, obtained from a pressure correction solution of a pseudo-Poisson equation, whose divergence is null.

In these capillary flows, care needs to be taken in the calculation of the capillary force $\mathbf{F}_{\sigma,s}$. The numerical method used to solve the interfacial force is the Continuum Surface Force (CSF) proposed by Brackbill (1992). The localization of the interface is available through a non-zero gradient of the volume fraction and the curvature is calculated from the volume fraction gradient. Thus, the surface force $\mathbf{F}_{\sigma,s}$ is transformed into a volume force $\mathbf{F}_{\sigma,v}$ by distributing its effects over grid points in the vicinity of the interface in a region that is a few cells thick: $\mathbf{F}_{\sigma,v} = -\sigma \nabla \cdot (\nabla C / \|\nabla C\|) \nabla C$.

Throughout this study, only a quarter of the channel is considered since the effects due to gravity in microchannels can be neglected ($Bo \leq 0.1$). The bubble is placed in the domain and a pressure gradient between two periodic boundary conditions is imposed to induce the motion until the flow reaches a steady state. No-slip wall conditions are imposed on the

planes $x = w$ and $y = h$ while a symmetry boundary condition is set at $x=0$ and $y=0$. The grids used consist of $32 \times 32 \times 256$, $48 \times 32 \times 256$ and $64 \times 32 \times 256$ cells for microchannels with aspect ratios of 1, 2.5 and 4, respectively. In order to correctly resolve the thin liquid film between the bubble and the wall, these grids are refined at the walls using a geometric evolution that decreases cell size in the last 32 cells in the x and y directions. In the axial direction, a regular grid spacing is used and the length of the unit cell is $17 \times h$. The parameters considered in this study have been chosen so that the Laplace number $La = Re/Ca = \rho_L D_h \sigma / \mu^2$ is constant in all the geometries and equal to $La = 280$. The ratios of liquid to gas densities and viscosities have been set to $\rho_L / \rho_G = 10^3 = \mu_L / \mu_G$.

3. Results and discussion

In this section, the results concerning global observations about recirculation patterns, shapes of the recirculation zone in a cross-section of the slug, recirculating volumes, as well as recirculation times are given. As shown theoretically in circular channels (Thulasidas et al., 1997), the recirculation characteristics of infinite slugs can be related to one parameter, which is the slip velocity $W = (U_B - U_{TP}) / U_B$. Many studies dealing with the dynamics of gas–liquid Taylor flow relate W to the capillary number (Bretherton, 1961; Aussillous and Quéré, 2000). In this study, the flow conditions were modified by varying the capillary number in the range $0.04 \leq Ca_B \leq 0.5$ and the corresponding Reynolds number in the range $11.2 \leq Re_B \leq 140$ whilst keeping the gas void fraction constant at 31%.

To study the effects of slug length on the recirculation characteristics, the geometry with an aspect ratio $\alpha = 2.5$ has been considered and the capillary number has been set to $Ca = 0.1 + / - 0.0005$ that leads to $W = 0.3303 + / - 0.0021$. Five different cases have been simulated by varying slug length from $2.90 \times h$ to $20.06 \times h$ and the corresponding volume fraction of gas phase ranges from 50% to 12.5%.

3.1. Recirculation pattern and local velocity field

The recirculation patterns in a rectangular channel with aspect ratio $\alpha = 2.5$ with varying capillary numbers are shown in Fig. 2. The local velocity field is shown in terms of local liquid Peclet number $Pe_l = Re \times Sc = |U_l| D_h / D_L$ where $|U_l|$ is the local velocity magnitude in the frame of reference moving with the bubble, D_L is the mass diffusivity in the liquid and Sc is the Schmidt number and is set to 1.

It can be seen in Fig. 2 that the maximum value of the local Peclet number is found in the liquid film between the bubble rear cap and the wall. Whatever the capillary number, the maximum value of the local Peclet number in the liquid slug is found close to the wall, decreases to zero at the center of the recirculation loop and then increases whilst approaching the center of the channel. Furthermore, as the Reynolds number increases, the boundary layer close to the bubble caps (where the Peclet number is very low) decreases in size. It can also be seen that recirculation loops through both the channel width and depth are formed. However, as the capillary number increases, the recirculation pattern in the less confined direction (channel width) diminishes until the closed loop is entirely lost. These changes in the streamline patterns are mainly observable in the wake of the bubble where the flow is particularly disturbed and the streamlines do not follow the shape of the rear of the bubble in the less confined direction.

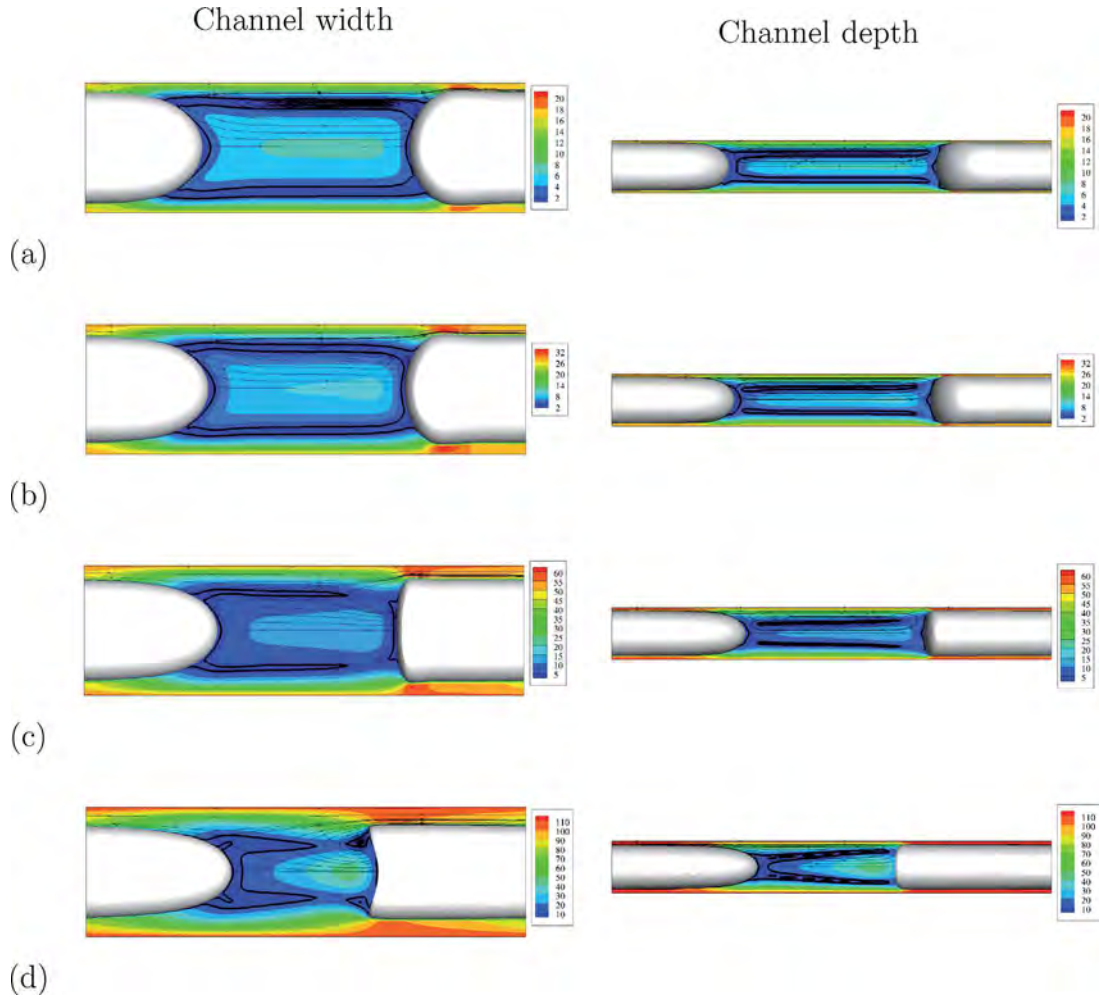


Fig. 2 – Local liquid Peclet numbers and streamlines through the channel width and depth for channel aspect ratio of 2.5. (a) $Ca = 0.06$, $Re = 16.8$; (b) $Ca = 0.1$, $Re = 28$; (c) $Ca = 0.2$, $Re = 56$; (d) $Ca = 0.4$, $Re = 112$. The bold line represents a Peclet number of 2 for (a)–(c) and 10 for (d) where $Ca = 0.4$ and $Re = 112$.

These observations also depend strongly on the cross-sectional shape of the channel and it can be seen in Fig. 3 that the detachment of the streamlines is enhanced when the aspect ratio increases. Indeed, although the recirculation loop in the square geometry seems qualitatively similar to that in a circular geometry, strong 3-dimensional effects of the rectangular geometry on the velocity field in the wake of the bubble are observed. In addition to the streamline pattern in the wake of the bubble, the same phenomenon is observed at the front cap of the bubble in the very wide shallow channel (aspect ratio $\alpha = 4$). This is in agreement with previous works on semi-infinite bubbles at low Reynolds numbers (Hazel and Heil, 2002) in rectangular channels.

The effects of the capillary number and the aspect ratio on the dimensionless velocity at the channel centerline is illustrated in Fig. 4 and 5 respectively. It is seen that close to the bubble caps, the velocity at the channel centerline increases from the bubble velocity to the maximum velocity expected in the liquid slug that depends on the mean velocity (from Eqs. (1) and (2), $U_{max} \sim [2.10; 1.92; 1.77] \times U_{TP}$ for channel cross-sections of aspect ratios $\alpha = [1; 2.5; 4]$). It is also observed (Figs. 4 and 5) that as the capillary number increases or the aspect ratio increases, there is a region in the wake of the bubble where the liquid velocity is greater than the maximum velocity of a laminar single-phase flow close to bubbles caps.

These observation suggest that the recirculation characteristics are not only governed by the dimensionless slip velocity

W but also by the slug length and this will be discussed in detail in Sections 3.3 and 3.4. The influence of slug length is expected when the development lengths at the rear and front caps of the bubbles are non negligible in comparison with the slug length, as illustrated with the streamlines and local Peclet numbers in Figs. 2 and 3.

3.2. Shape of the recirculation zone

The cross-sectional area occupied by the recirculation zones as approximated by the theoretical fully-developed velocity profile (see Section 2.1) has been calculated and is shown in Fig. 6 for the three aspect ratios: $\alpha = [1; 2.5; 4]$. It can be seen that the recirculation areas follow the shape of the channel for low dimensionless velocities and reduce to circular and elliptical shapes as the velocity (or Ca) increases.

When the channel aspect ratio increases, the aspect ratio of the recirculation zone also increases. Furthermore, the center of the recirculation loop and the separating streamline both move faster towards the center of the channel in the less confined direction. As a result, the slug film thickness is greater in the width of the microchannel than in the height.

Mass transfer between the film and the recirculating regions will occur by molecular diffusion through the interface separating these regions. In a 2-dimensional representation through the channel cross-section, the perimeter that separates the recirculating and film regions can be used to

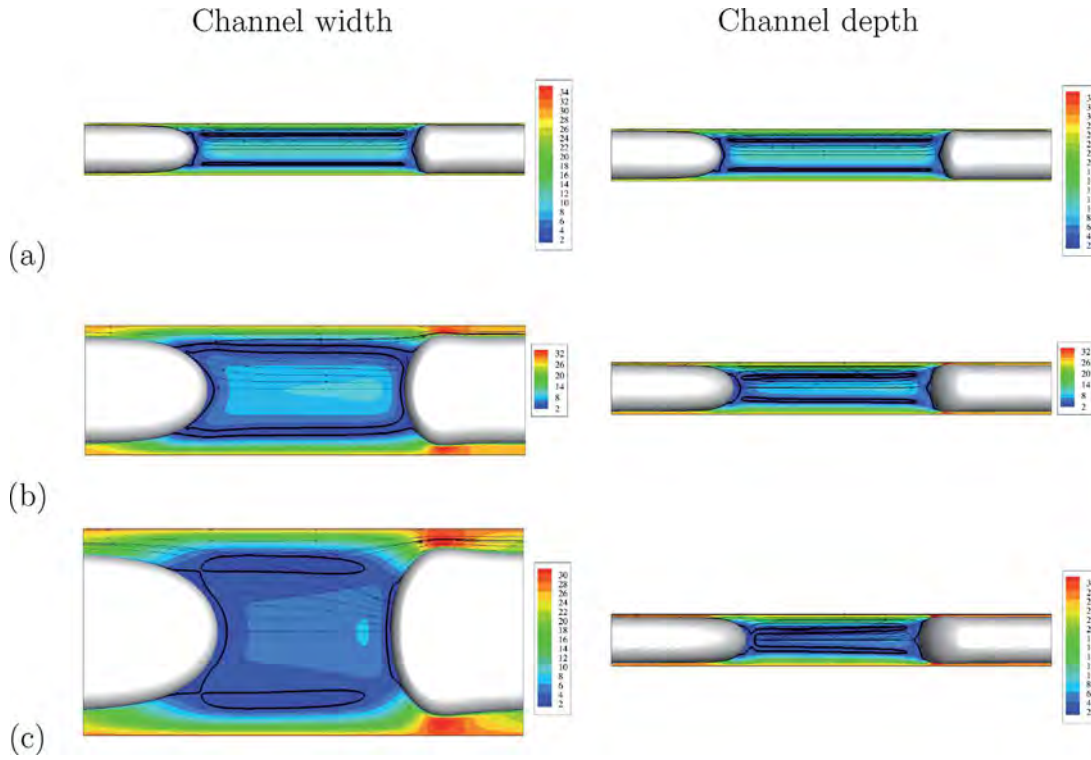


Fig. 3 – Local liquid Peclet numbers and streamlines through the channel width and depth for $Ca = 0.1$ and $Re = 28$. (a) $\alpha = 1$; (b) $\alpha = 2.5$; (c) $\alpha = 4$. The bold line represents a Peclet number of 2.

understand transport processes between the recirculating and film regions. Fig. 7 shows the evolution of the perimeter that separates the recirculating and film regions in Fig. 6 as a function of the dimensionless slip velocity. To compare the three aspect ratios with circular channels, the perimeters are normalized by the perimeter of a circular channel with an equivalent hydraulic diameter D_h . It is clearly seen that the perimeter that links the recirculation zone and the film region is greater in square channels than in circular channels. As the aspect ratio increases, the perimeter that separates the

recirculating and film regions also increases until a certain velocity W above which the opposite trend is observed. The velocity at which the transition occurs decreases as the aspect ratio increases. As a consequence, it is expected that when dealing with wall to slug mass transfer, channels with a high aspect ratio will typically provide better mass transfer than channels with square or circular cross-section. However, mass transfer from the recirculation zone to the film will also depend on the time needed for a fluid element to travel the slug distance and more generally, mixing efficiency will

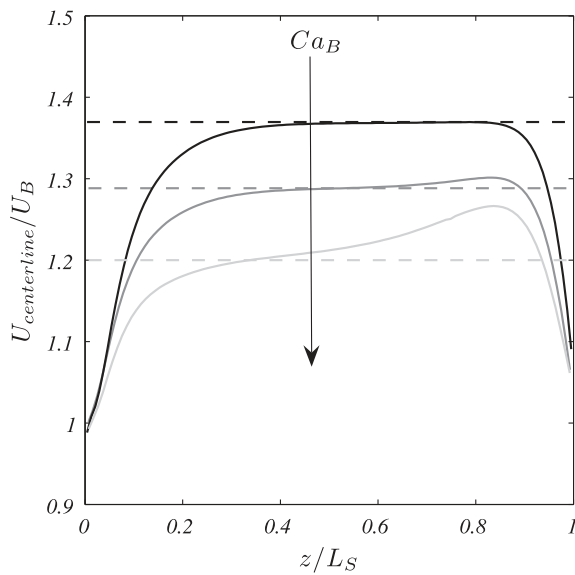


Fig. 4 – Dimensionless liquid velocity along the centerline of the channel between two bubbles for an aspect ratio of 2.5 and various capillary numbers. Legend: (—) $U_{centerline}/U_B$; (---) U_{max}/U_B evaluated from U_{TP} and Eqs. (1) and (2); (black) $Ca = 0.06$; (gray) $Ca = 0.1$; (light gray) $Ca = 0.2$.

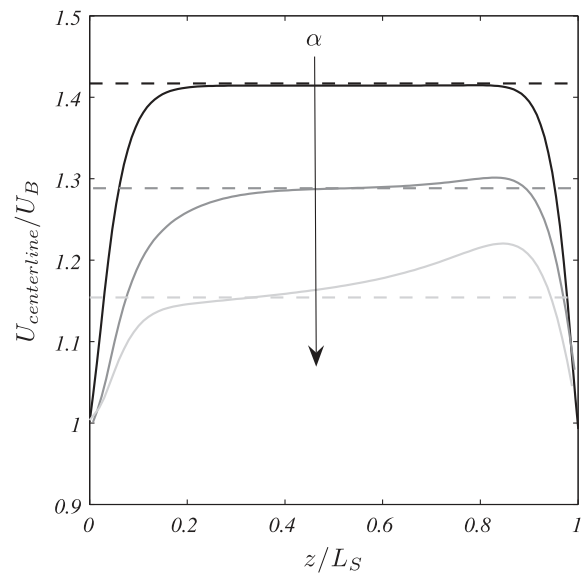


Fig. 5 – Dimensionless liquid velocity along the centerline of the channel between two bubbles for $Ca = 0.1$ and for aspect ratios 1, 2.5 and 4. Legend: (—) $U_{centerline}/U_B$; (---) U_{max}/U_B evaluated from U_{TP} and Eqs. (1) and (2); (black) $\alpha = 1$; (gray) $\alpha = 2.5$; (light gray) $\alpha = 4$.

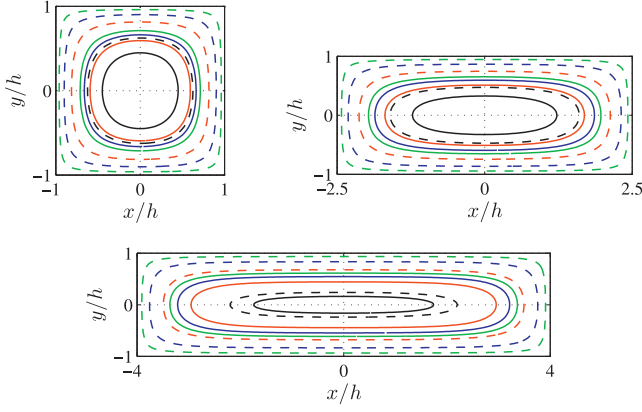


Fig. 6 – Cross-sectional shape of the recirculating zone for aspect ratios $\alpha = [1; 2.5; 4]$ for different dimensionless velocities W . Legend: (—) center of the recirculating loop; (---) streamline separating the circulation loop and the film. From the walls to the center (green; blue; red; black): $W = [0.1; 0.2; 0.3; 0.42]$. (For interpretation of the references to color in this figure legend, the reader is referred to the web version of the article.)

depend on the total recirculation time, as well as the size of the recirculating volume.

3.3. Characteristic recirculating volumes

A characteristic parameter of the recirculation motion in Taylor flow is the volume of fluid recirculating in the slug. Unlike in cylindrical tubes where the volumes of positive flow and negative flow of the recirculation region are equal, it is not the case in square and rectangular ducts. Indeed, in the channel cross-section the ratio of total recirculation area over positive recirculation area increases with the aspect ratio and tends to

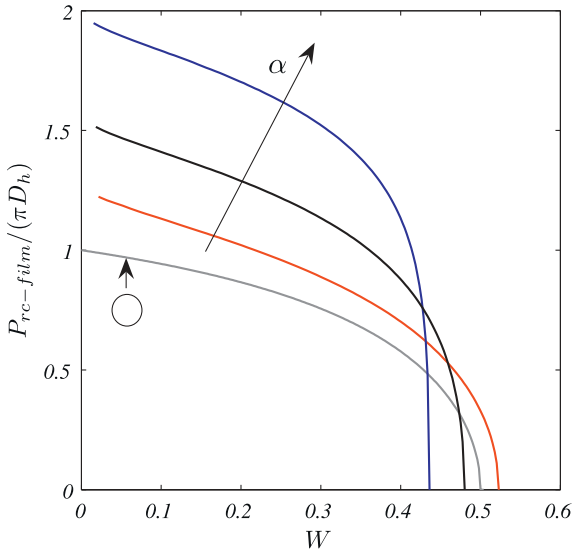


Fig. 7 – Perimeter of the recirculation zone through the channel cross-section (as depicted by dashed lines in Fig. 6) normalized by the perimeter of a circular channel with an equivalent hydraulic diameter D_h in a cross-section of the slug as a function of the dimensionless velocity W . Legend: (gray) circular channels; (red) $\alpha = 1$; (black) $\alpha = 2.5$; (blue) $\alpha = 4$. (For interpretation of the references to color in this figure legend, the reader is referred to the web version of the article.)

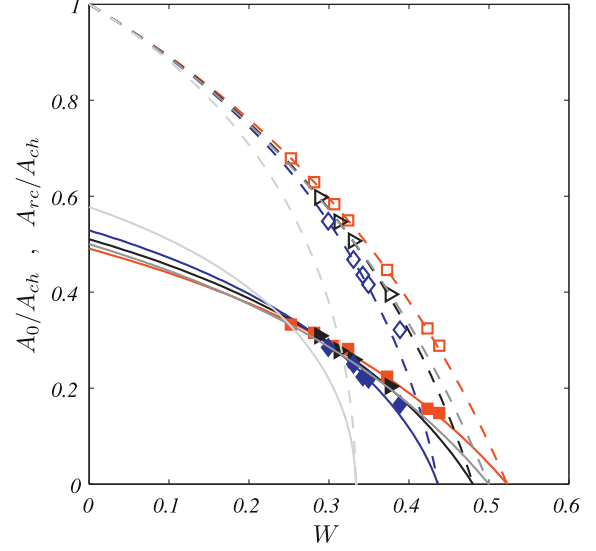


Fig. 8 – Dimensionless cross-section of the recirculating areas at the center of the slug versus the dimensionless bubble velocity. Legend: (—) A_0/A_{ch} , infinite slug length assumption; (---) A_{rc}/A_{ch} , infinite slug length assumption; (gray) circular channels; (light gray) 2D channels; (filled symbols) A_0/A_{ch} ; (open symbols) A_{rc}/A_{ch} ; (\square , red) $\alpha = 1$, numerical; (\blacktriangleright , black) $\alpha = 2.5$, numerical; (\diamond , blue) $\alpha = 4$, numerical. (For interpretation of the references to color in this figure legend, the reader is referred to the web version of the article.)

$\sqrt{3}$ for the asymptotic behavior of an infinite aspect ratio. In addition, for a fixed geometry, the ratio of recirculation areas also varies with the dimensionless velocity W .

The size of the recirculation area at the center of the slugs for channel aspect ratios $[1; 2.5; 4]$ are shown in Fig. 8. A_{rc} (cross-section of the recirculating liquid) and A_0 (cross-section of the positive part of the recirculating liquid) are normalized by the channel cross-section area A_{ch} . The results integrated from the analytical velocity profile corresponding to infinite slug length and the results obtained from the numerical simulations with finite slug length are compared and very good agreement between the computational and theoretical results is observed, as long as the liquid velocity profile is fully-developed at the center of the slug. The computations that show a slight deviation from the theory correspond to cases where the velocity profile is not entirely fully-developed at the center of the slug. For short slugs, the laminar velocity profile is not fully-developed and the region where the flow is disturbed by the bubble is not negligible; therefore the recirculating volumes and times cannot be approximated by the theoretical velocity profile. In such cases, the recirculating volume is obtained from direct numerical simulations by integrating small slices of recirculating zones along the slug.

Fig. 9 shows the influence of the slug length on the recirculating volume V_{rc} and the positive part of the recirculating volume V_0 normalized by the slug volume V_{slug} . In every simulation, care has been taken that the bubble is long enough and the dimensionless bubble velocity is constant whatever the slug and bubble lengths. From this data, it is clear that the regions close to bubble caps do not affect the ratio of recirculating volume over slug volume significantly.

Fig. 10 shows the ratio of the recirculating volumes V_0 and V_{rc} over total slug volume V_{slug} as a function of the capillary number for the three rectangular microchannel

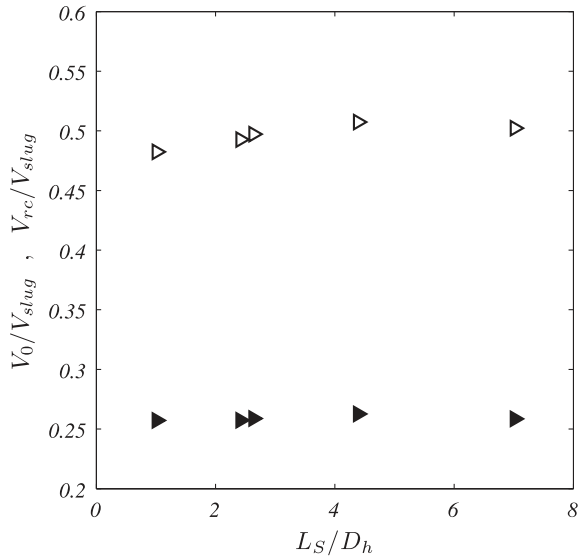


Fig. 9 – Dimensionless recirculation volumes as a function of dimensionless slug length. Legend: (filled symbols) V_0/V_{slug} ; (open symbols) V_{rc}/V_{slug} .

geometries. The recirculating volume for the infinite aspect ratio and axisymmetrical cases are also given using the relation $W=f(Ca)$ from [Aussillous and Quéré \(2000\)](#) for the tubes and [Abadie et al. \(2012\)](#) for 2D cases; both assume long liquid slug in order to neglect the changes in the flow close to the bubble caps. It should also be kept in mind that axisymmetrical and planar cases are given as an indication only since the relations $W=f(Ca)$ for these cases are valid for negligible inertia, which is not the case in the present work since $Re \geq 10$. Experimental data obtained by μ -PIV in [Zaloha et al. \(2012\)](#) (obtained for a Laplace number $La = Re/Ca \sim 1000$) are also presented. As expected, the recirculating volumes are close to the slug volume at low capillary numbers ($Ca_B \sim 10^{-3}$) due to the fact that the bypass flow is negligible compared

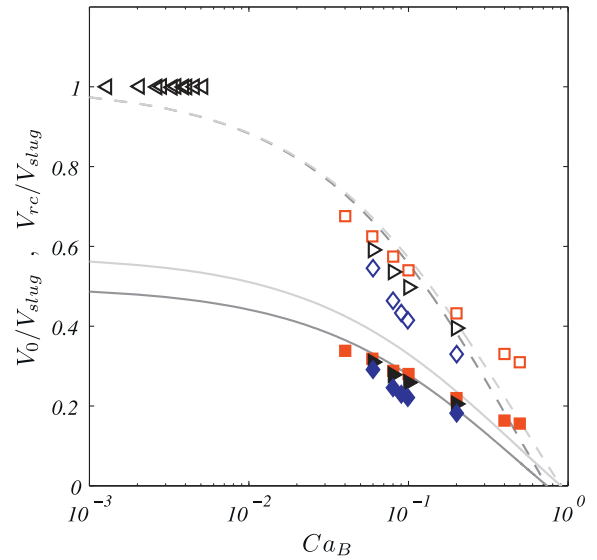


Fig. 10 – Dimensionless recirculating volume as a function of the capillary number. Legend: (—) V_0/V_{slug} , infinite slug length assumption; (—) V_{rc}/V_{slug} , infinite slug length assumption; (gray) circular channels; (light gray) 2D channels; (filled symbols) V_0/V_{slug} ; (open symbols) V_{rc}/V_{slug} ; (\triangleleft , black) $\alpha = 2.5$, experimental ([Zaloha et al., 2012](#)); (\square , red) $\alpha = 1$, numerical; (\triangleright , black) $\alpha = 2.5$, numerical; (\diamond , blue) $\alpha = 4$, numerical. (For interpretation of the references to color in this figure legend, the reader is referred to the web version of the article.)

with the total flow rate. In other words, almost all the liquid contributes to the recirculation motion. Then, as the capillary number increases, the recirculating volume significantly decreases in all the geometries. Although the volume of the positive recirculating flow is hardly dependent on the geometry, the total recirculating volume decreases as the aspect ratio increases.

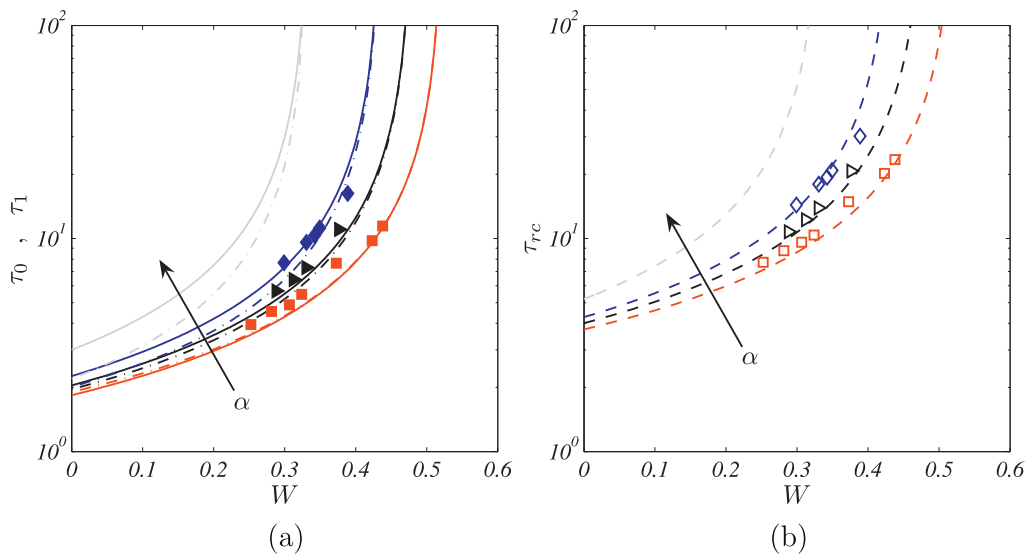


Fig. 11 – (a) Dimensionless recirculation times τ_0 and τ_1 versus the dimensionless bubble velocity. Legend: (—) τ_0 , infinite slug length assumption; (---) τ_1 , infinite slug length assumption; (light gray) 2D channels; (filled symbols) τ_0 , numerical (\square , red) $\alpha = 1$; (\triangleright , black) $\alpha = 2.5$; (\diamond , blue) $\alpha = 4$. (b) Dimensionless total recirculation time τ_{rc} versus the dimensionless bubble velocity. Legend: (---) τ_{rc} , infinite slug length assumption; (light gray) 2D channels; (open symbols) τ_{rc} , numerical; (\square , red) $\alpha = 1$; (\triangleright , black) $\alpha = 2.5$; (\diamond , blue) $\alpha = 4$. (For interpretation of the references to color in this figure legend, the reader is referred to the web version of the article.)

3.4. Characteristic recirculation times

The characteristic recirculation times τ_0 for the positive recirculation flow, τ_1 for the negative flow and τ_{rc} for the total recirculation as a function of the dimensionless velocity are plotted in Fig. 11 in comparison with the infinite slug length assumption. The effects of slug length on positive (τ_0) and total (τ_{rc}) recirculation times are represented in Fig. 12 and the recirculation times as a function of the capillary number are then plotted in Fig. 13.

Although the recirculation areas show very good agreement with the theoretical predictions, the recirculation times τ_{rc} are greater than those determined using the infinite slug assumption (Fig. 11), and mainly for aspect ratios 1 and 2.5 at low capillary numbers. Indeed, close to bubble caps where the flow is disturbed, the axial flow rate is reduced and the recirculation time is increased. However, as the capillary number or the aspect ratio increase, the velocity in the wake of the bubble increases (see Figs. 4 and 5) and balances the lower velocities in the vicinity of the interface. It can be seen in Fig. 11 that the recirculation time for the channel with aspect ratio of 4 (represented with diamonds in blue) is lower in our calculations compared with the infinite slug assumption. The trends observed for all geometries are qualitatively similar and an increase in the aspect ratio leads to an increase in both the positive and negative recirculation times and thus in the total recirculation time until divergence when complete by-pass flow is attained.

Although the recirculating volume only depends on the dimensionless velocity W , it is shown in Fig. 12(a) that the dimensionless recirculating times vary with the slug length. Indeed, whilst the disturbed flow around the bubble does not change the recirculating volume, it does cause an increase in the recirculation time when the slug length decreases, as mentioned in the previous paragraph. As expected, the recirculation times tend towards the value evaluated from the theoretical laminar single-phase flow representing the case of an infinite slug length. For the shortest slug considered here, the total recirculation time is 20% longer than the asymptotic value. Leung et al. (2010) studied the effect of slug length on the Nusselt number with a constant heat flux on the wall of a circular tube and found an increase in the Nusselt number as the slug length decreases. Indeed, fluid elements will refresh the interface separating the recirculating and film regions more frequently in short slugs. The evolution of the mean time for a fluid element to complete a cycle can be represented in a dimensional form to illustrate this decrease in recirculation time as the slug length decreases. It is seen in Fig. 12(b) that although the recirculation time is slightly underestimated with the infinite slug length assumption due to the increased time taken for a fluid element to travel the development length close to bubble caps, the recirculation time decreases as the slug length decreases.

In the cases presenting a recirculation motion in the liquid slug, the bubble velocity is lower than the liquid velocity at the centerline of the channel. Thus, around the bubble caps, there is a region where the velocity on the channel centerline decreases to the bubble velocity, as shown in Figs. 4 and 5. This explains the increase in recirculation time when the slug length decreases since the ratio of development length over slug length increases.

Here, it has been observed that in the development region close to the bubble caps, the centerline velocity can be greater than the expected velocity on the axis (e.g. $U_{max} = 1.92 \times U_{TP}$

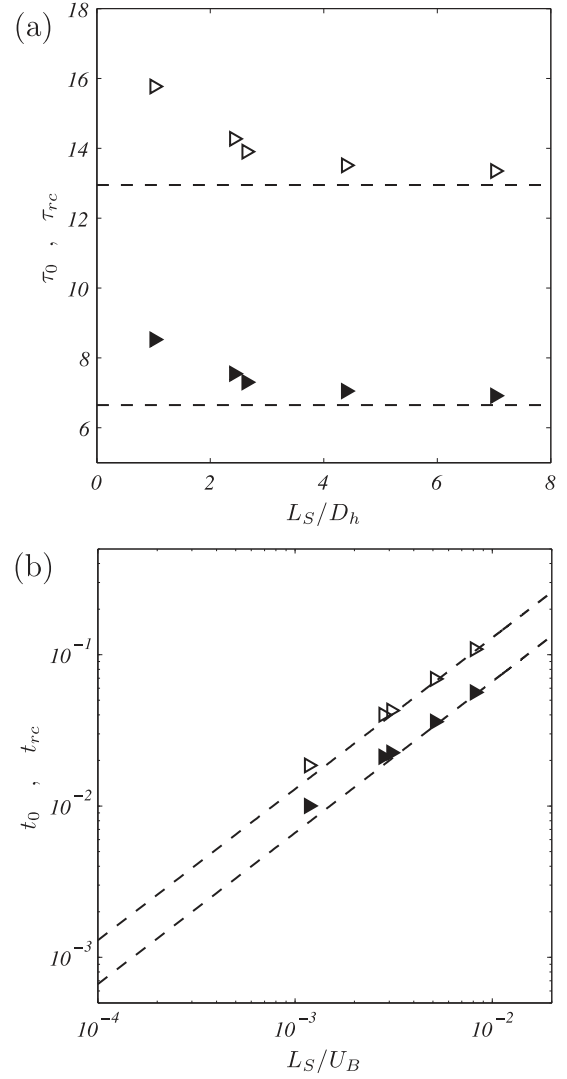


Fig. 12 – (a) Dimensionless recirculation times as a function of dimensionless slug length. Legend: (—) asymptotic values τ_0 and τ_{rc} ; (filled symbols) τ_0 ; (open symbols) τ_{rc} . (b) Dimensional recirculation times t_0 and t_{rc} (with $D_h = 571 \mu\text{m}$ and $U_B = 0.5 \text{ m/s}$) as a function of the time taken for a bubble to travel the slug length L_S/U_B . Legend: (—) asymptotic values t_0 and t_{rc} ; (filled symbols) t_0 ; (open symbols) t_{rc} .

for the 2.5 aspect ratio channel, Fig. 4 for $Ca \geq 0.1$) before stabilizing if the slug is long enough. This local increase in the velocity can lead to a decrease in the recirculation time as the slug length decreases. This phenomenon is accentuated as the aspect ratio increases and it can be seen in Fig. 11 that recirculation times evaluated in the numerical simulations are lower than that for an infinite slug length with the aspect ratio 4 and $W > 0.3$.

Fig. 13 reports the evolution of the recirculation times as a function of the capillary number. It is shown that an increase in the capillary number also leads to an increase in the recirculation time for all the geometries considered. Thus, when the capillary number increases, the volume involved in the recirculation motion is reduced but the dimensionless time needed for a fluid element to travel the slug length is increased. It is also observed that the 2D theory is not a good approximation for high aspect ratios. In addition, it can be seen that even if the recirculating volume shows a weak dependency on the channel geometry, the effect observed on the recirculation time is more significant. Indeed, at fixed operating conditions (Ca , Re

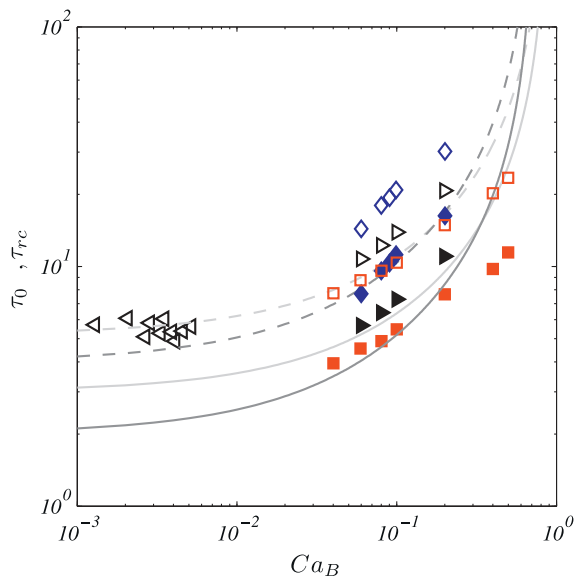


Fig. 13 – Dimensionless recirculation times versus the capillary number. Legend: (—) τ_0 , infinite slug length assumption; (---) τ_{rc} , infinite slug length assumption; (gray) circular channels; (light gray) 2D channels; (filled symbols) τ_0 ; (open symbols) τ_{rc} ; (\blacktriangleleft , black) $\alpha = 2.5$, experimental (Zaloha et al., 2012); (\square , red) $\alpha = 1$; (\blacktriangleright , black) $\alpha = 2.5$; (\diamond , blue) $\alpha = 4$, numerical. (For interpretation of the references to color in this figure legend, the reader is referred to the web version of the article.)

and L_S), an increase in the aspect ratio leads to significantly longer recirculation times.

4. Concluding remarks

Direct numerical simulations of gas–liquid Taylor flow in microchannels have been performed. The effects of channel cross-section and operating conditions on mixing and recirculation in the liquid slug have been investigated. The results of the numerical simulations have been compared with theoretical approximations for the case of infinite slug length in terms of cross-sectional recirculation area, recirculating volume and recirculation times. It has been shown that as long as the slug is long, the recirculation area in the slug can be well predicted using the fully-developed velocity profile. Whatever the geometry, increasing the capillary number leads to a decrease in recirculating volume and an increase in recirculation time, which means that transport processes will be hindered. Radial mixing is then reduced while axial dispersion is enhanced with increasing the capillary number. It has been shown that when the aspect ratio increases for a given capillary number, the recirculating volume decreases slightly and the recirculation time increases while the exchange surface between film and recirculating regions is enhanced at low slip velocities, which is the case for capillary numbers lower than approximately $Ca \sim 0.1$. Indeed, high aspect ratio channels may appear attractive for heat transfer in plate microreactors, however the decrease in the recirculation rate and effective recirculation volume is disadvantageous for both heat and mass transfer operations. It is therefore expected that some intermediate aspect ratio geometry would be most effective. This would require a systematic study that investigates the effects of process parameters (aspect ratio, void fraction, capillary number, Reynolds number) on the efficiency of the gas–liquid system

that could be expressed by a cost-function integrating global parameters (pressure drop, circulation volumes and times, mass transfer, heat transfer).

The disturbed flow close to the bubble caps has shown to generally increase recirculation time. It has also been shown that for certain cases in rectangular channels, the bubble wake causes a local increase in the velocity at the center of the channel and this phenomenon is enhanced in high aspect ratio channels and high capillary number flows. Although this increase in the axial velocity can lead to a slight decrease in the recirculation time, these wake effects do not balance geometrical effects and the recirculation times in wide shallow channels remain greater than the ones obtained in channels of lower aspect ratio.

Acknowledgements

This work was financed by the French “Agence Nationale de la Recherche” in the framework of the project MIGALI no. ANR-09-BLAN-0381-01. We also acknowledge the support from this project from the CNRS research federation FERMaT, such as the CALMIP, IDRIS and CINES projects for providing computational resources.

References

- Abadie, T., Aubin, J., Legendre, D., Xuereb, C., 2012]. Hydrodynamics of gas–liquid Taylor flow in rectangular microchannels. *Microfluid. Nanofluid.* 12, 355–369.
- Aussillous, P., Quéré, D., 2000]. Quick deposition of a fluid on the wall of a tube. *Phys. Fluids* 12, 2367–2371.
- Bonometti, T., Magnaudet, J., 2007]. An interface-capturing method for incompressible two-phase flows. validation and application to bubble dynamics. *Int. J. Multiphase Flow* 33, 109–133.
- Brackbill, J., Kothe, D.B.C.Z., C, Z., 1992]. A continuum method for modeling surface tension. *J. Comput. Phys.* 100, 335–354.
- Bretherton, F.P., 1961]. The motion of long bubbles in tubes. *J. Fluid Mech.* 10, 166–188.
- Dupont, J.B., Legendre, D., 2010]. Numerical simulation of static and sliding drop with contact angle hysteresis. *J. Comput. Phys.* 229, 2453–2478.
- Gupta, R., Fletcher, D.F., Haynes, B.S., 2010]. Taylor flow in microchannels: a review of experimental and computational work. *J. Comput. Multi. Flow* 2, 1.
- Hazel, A.L., Heil, M., 2002]. The steady propagation of a semi-infinite bubble into a tube of elliptical or rectangular cross-section. *J. Fluid Mech.* 470, 91–114.
- Hessel, V., Angeli, P., Gavriilidis, A., 2005]. Gas–liquid and gas–liquid–solid microstructured reactors: contacting principles and applications. *Ind. Eng. Chem. Res.* 44, 9750.
- Jaworski, Z., Nienow, A.W., Dyster, K.N., 1996]. An LDA study of the turbulent flow field in a baffled vessel agitated by an axial, down-pumping hydrofoil impeller. *Can. J. Chem. Eng.* 74, 3–15.
- Kashid, M.H., Kiwi-Minsker, L., 2009]. Microstructured reactors for multiphase reactions: state of the art. *Ind. Eng. Chem. Res.* 48, 6465–6485.
- Kececi, S., Worner, M., Onea, A., Soyhan, H.S., 2009]. Recirculation time and liquid slug mass transfer in co-current upward and downward Taylor flow. *Catal. Today* 147S, S125–S131.
- Kreutzer, M.T., Kapteijn, F., Moulijn, J.A., Heizwolf, J.J., 2005]. Multiphase monolith reactors: chemical reaction engineering of segmented flows in microchannels. *Chem. Eng. Sci.* 60, 5895–5916.
- Leung, S.S.Y., Liu, Y., Fletcher, D.F., Haynes, B.S., 2010]. Heat transfer in well-characterised Taylor flow. *Chem. Eng. Sci.* 65, 6379–6388.

- Sarrazin, F., Bonometti, T., Loubière, K., Prat, L., Gourdon, C., Magnaudet, J., 2006a]. [Experimental and numerical study of droplets hydrodynamics in microchannels](#). *AIChE J.* 52, 4061–4070.
- Sarrazin, F., Bonometti, T., Loubière, K., Prat, L., Gourdon, C., Magnaudet, J., 2006b]. [Hydrodynamics structures of droplets engineered in rectangular microchannels](#). *Microfluid. Nanofluid.* 5, 131–137.
- Shao, N., Gavriilidis, A., Angeli, P., 2009]. [Flow regimes for adiabatic gas–liquid flow in microchannels](#). *Chem. Eng. Sci.* 64, 2749–2761.
- Taylor, G.I., 1961]. [Deposition of a viscous fluid on the wall of a tube](#). *J. Fluid Mech.* 10, 161–165.
- Thulasidas, T.C., Abraham, M.A., Cerro, R.L., 1997]. [Flow patterns in liquid slugs during bubble-train flow inside capillaries](#). *Chem. Eng. Sci.* 52, 2947–2962.
- Zalesak, S.T., 1979]. [Fully multidimensional flux-corrected transport algorithms for fluids](#). *J. Comput. Phys.* 31, 335–362.
- Zaloha, P., Kristal, J., Jiricny, V., Volkel, N., Xuereb, C., Aubin, J., 2012]. [Characteristics of liquid slugs in gas–liquid Taylor flow in microchannels](#). *Chem. Eng. Sci.* 68, 640–649.